Energy Storage Materials 84 (2026) 104784

Contents lists available at ScienceDirect

Energy Storage Materials

journal homepage: www.elsevier.com/locate/ensm

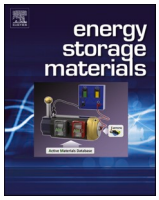

Aromatic thioamide cathode with reversible C=S-centered multielectron redox for high-capacity Li-Ion storage

Tingting Jiang [a], Wenwen Deng [a,b,c,*], Qingqing Ma [b], Chunxian Guo [a,*], Zhong Jin [c,*]

[a] School of Material Science and Engineering, Suzhou University of Science and Technology, Suzhou 215000, China
[b] School of Materials Science and Engineering, Anhui University, 230601 Hefei, Anhui, PR China
[c] State Key Laboratory of Coordination Chemistry, MOE Key Laboratory of Mesoscopic Chemistry, MOE Key Laboratory of High Performance Polymer Materials and Technology, Jiangsu Key Laboratory of Clean Energy Catalysis and Intelligent Green Chemical Engineering, Suzhou Key Laboratory of Green Intelligent Manufacturing of New Energy Materials and Devices, Tianchang New Materials and Energy Technologies Research Center, Institute of Green Chemistry and Engineering, School of Chemistry and Chemical Engineering, Nanjing University, Nanjing, Jiangsu 210023, China

ARTICLE INFO

Keywords:
Lithium-ion batteries
Organic sulfide cathode
C=S-centered redox electrochemistry
Thioamide

ABSTRACT

Organic sulfur–based cathodes have attracted broad interest for lithium-ion batteries owing to their high theoretical capacities and structural diversity. Conventional organosulfides achieve multielectron redox electrochemistry via reversible S–S bond cleavage, but this pathway suffers from sluggish kinetics, low energy efficiency, and dissolution-driven capacity fade. Here we report a thioamide-based organic cathode, benzene-1,4-dithiocarboxamide (BDTA), that enables a four-electron redox process exclusively through reversible cleavage and reformation of C=S bonds—a scarcely explored motif in lithium-battery chemistry. BDTA delivers an initial capacity of 543 mAh g^{-1}, approaching the theoretical value for a four-electron transfer, and maintains 354 mAh g^{-1} after 50 cycles. In situ Fourier-transform infrared (FTIR) and ex situ x ray photoelectron spectroscopy (XPS) confirm the reversible interconversion between C=S and C–S bonds during (de)lithiation and reveal synergistic electronic contributions from adjacent C–N groups that stabilize the redox centers. Complementary Gaussian calculations elucidate the stepwise Li^{+} binding sequence. Extending this concept, naphthalene-1,4-dithiocarboxamide (NDTA) demonstrates that C=S-centered redox electrochemistry can be transferable from benzene to naphthalene frameworks. Our work establishes a thioamide-driven redox paradigm and provide a design blueprint for high-capacity, multielectron organic cathodes beyond conventional S–S-bonded reswsystems.

1. Introduction

With the accelerating global transition toward carbon neutrality, the development of high–energy-density energy storage technologies have become essential for supporting electric vehicles and smart grid systems. Despite broad use, LIBs remain capped in energy density by the <250 mAh g^{-1} theoretical limit of transition-metal oxide cathodes and by the constrained availability of their constituent metals [1]. To address this challenge, alternative cathode materials with higher specific capacities and sustainable resources are urgently needed [2–4].

Organic electrode materials (OEMs) have garnered growing interest as promising alternatives due to their structural diversity, environmental friendliness, and potential for high capacity. Among them, organosulfides, which undergo multielectron redox reactions through the reversible cleavage and formation of S–S bonds, offer intrinsically high charge-storage density per molecule and a tunable molecular platform for designing high-energy cathodes [5–7]. Most reported organosulfur cathodes rely on a storage pathway based on the reversible cleavage and reformation of S–S bonds [8–10]. However, this pathway involves multiphase intermediates and multistep transformations, resulting in an elongated reaction route and sluggish kinetics, thereby weakening reaction reversibility and energy efficiency [11]. Moreover, the discharge end product Li_2S tends to deposit irreversibly on the cathode surface, leading to electrode passivation and capacity loss [12]; meanwhile, soluble lithium polysulfide (LiPS) intermediates undergo dissolution–shuttling, causing active-material loss, anode corrosion, and reduced coulombic efficiency—effects that are further aggravated at elevated temperatures and ultimately limit cycling stability [13].

* Corresponding authors.
E-mail addresses: 24177@ahu.edu.cn (W. Deng), cxguo@usts.edu.cn (C. Guo), zhongjin@nju.edu.cn (Z. Jin).

https://doi.org/10.1016/j.ensm.2025.104784
Received 14 October 2025; Received in revised form 24 November 2025; Accepted 29 November 2025
Available online 1 December 2025
2405-8297/© 2025 Elsevier B.V. All rights are reserved, including those for text and data mining, AI training, and similar technologies.

Although polymerization [14], carbon confinement [15], and hybrid composite design [16,17] can mitigate dissolution and shuttling, the associated synthetic complexity constrain scalability and deliver limited improvements. For example, long-chain (n > 2) organosulfur molecules are often difficult to synthesize and purify to analytical grade, and some are air-sensitive, increasing challenges in storage and handling [18]. In addition, structural rearrangement/aggregation (e.g., isomerization and di-/tri-/tetramerization) [19] may also occur during cycling, further complicating the product spectrum and undermining controllability and reversibility.

In view of these issues, there is an urgent need to replace S–S–dominated pathways with more stable, reversible, and kinetically favorable bond-centered redox electrochemistry, thereby mitigating shuttle, deposition, and polarization at the source.

In this context, we turn our attention to thioamide-based compounds, a largely unexplored subclass of sulfur-containing organics featuring C=S bonds instead of S–S moieties. A new compound benzene-1,4-dithiocarboxamide (BDTA) was synthesized as a new type of organic cathode for rechargeable lithium batteries. Through comprehensive electrochemical characterizations, we demonstrate that BDTA enables a four-electron redox process through reversible C=S bond cleavage and reformation, delivering an initial capacity of 543mAh g^{-1}, and excellent cycling stability. In-depth mechanistic investigations, combining in situ FTIR, ex situ XPS, and Gaussian calculations, elucidate the lithium-storage pathway and reveal the synergistic roles of C=S and adjacent C–N groups in facilitating multielectron reactions. Building on this concept, naphthalene-1,4-dithiocarboxamide (NDTA) shows that C=S-centered redox electrochemistry is not confined to benzene, but translates to a naphthalene scaffold. This work introduces a redox paradigm based on C=S-centered thioamide chemistry, offering an alternative to traditional S–S-based organosulfides and expanding the molecular toolbox for high-capacity organic cathode design.

2. Results and discussion

To highlight the structural merits of the thioamide motif, we benchmarked BDTA against a representative organic disulfide, dipyridine disulfide (DPyDS). DPyDS was chosen because it shares an N–C–S framework but employs an S–S single bond as the redox-active center, enabling a direct comparison with BDTA's C=S double bond in terms of redox reactivity and Li-storage performance. HOMO–LUMO calculations (Fig. 1**a**) show that BDTA has a much narrower gap (Eg = 3.69 eV) than DPyDS (Eg = 5.40 eV), indicative of greater electronic delocalization and enabling more efficient electron transfer during charge–discharge [20–22]. ESP mapping inFig. 1**b** reveals two concentrated, symmetric minima around the C=S groups in BDTA (≈ −32.11 and −30.07), whereas DPyDS exhibits more dispersed negative regions (≈ −40.34 and −26.62). These well-defined minima mark the C=S sites as preferred Li^+ anchoring and redox-active centers, thereby enabling more efficient Li storage [23]. Additionally, lithiation Gibbs free energies (ΔG) were computed for BDTA and DPyDS (Fig. 1**c**). As shown, BDTA shows a much more negative ΔG (−353.29 kJ mol^{-1}) than DPyDS (−252.82 kJ mol^{-1}), indicating thermodynamically more favorable lithiation with facile activation of the C=S bonds. Accordingly, C=S-centered BDTA outperforms S–S–based analogues in both electronic structure and thermodynamic favorability, providing a superior molecular platform for efficient multielectron Li storage. Motivated by these advantages, we conducted an in-depth investigation of BDTA's structure, electrochemical performance, and reaction mechanism.

BDTA was obtained by reacting 1,4-dicyanobenzene with 50 wt % ammonium sulfide aqueous solution at room temperature for 30 min, [24] and finally a pale yellow powdery product is obtained (Fig. 2**a**). To

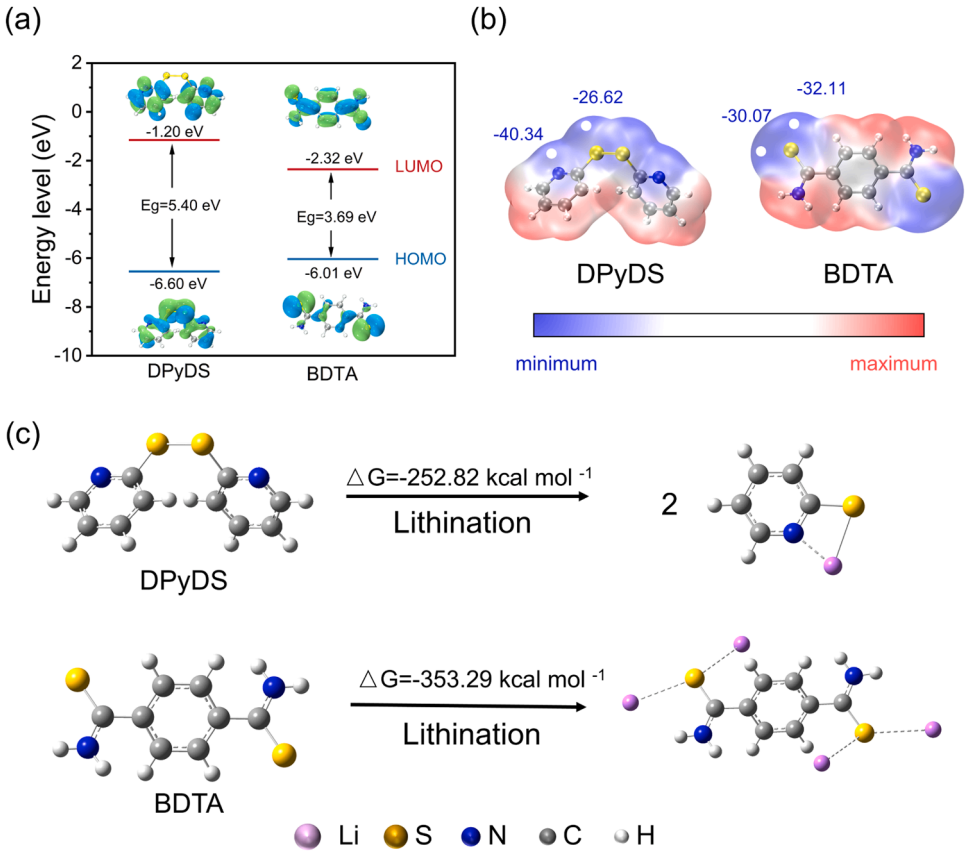

Fig. 1. Gaussian calculations about: (a) LUMO—HOMO energy level diagram; (b) ESP analysis; (c) Lithiation path and calculation of Gibbs free energy for the lithiation process of BDTA and DPyDS.

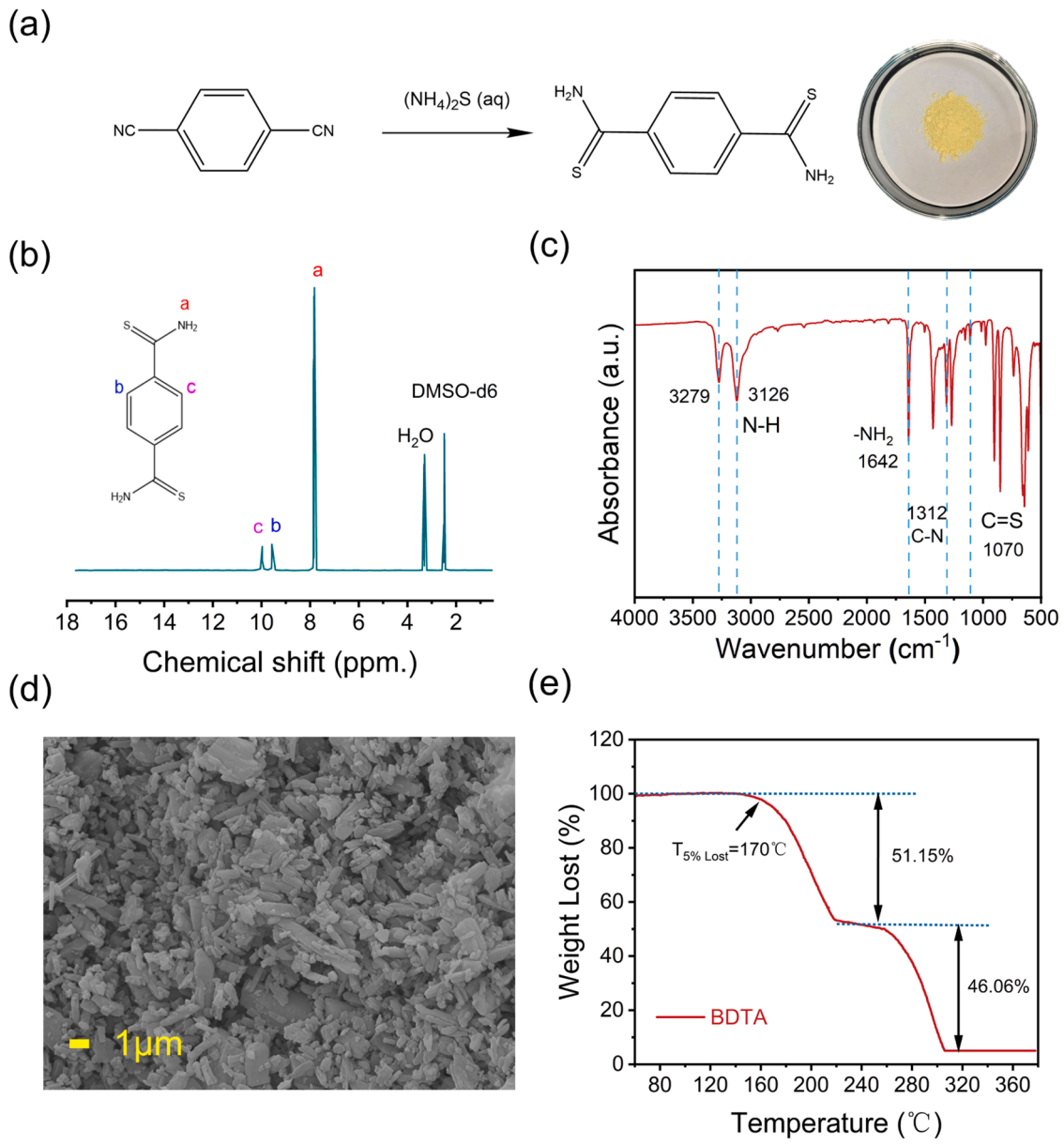

Fig. 2. (a) Synthetic route of BDTA and photograph of the obtained product; (b) ^{1}H NMR spectrum of BDTA (solvent: DMSO-d_6); (c) FTIR spectrum of BDTA with characteristic absorption peaks of functional groups labeled; (d) SEM image of BDTA; (e) Thermogravimetric analysis (TGA) curve of BDTA.

verify the structure and physicochemical identity of the product, BDTA was systematically characterized. The ^{1}H NMR spectrum (Fig. 2**b**) shows three characteristic resonances assigned to the amide –NH_2 (a) and aromatic protons (b, c), confirming successful synthesis. FTIR (Fig. 2**c**) further substantiates the thioamide functionality, with distinct bands at 3279 and 3126 cm^{-1} (ν(N–H)), 1642 cm^{-1} (δ(NH_2)) [20], 1312 cm^{-1} (ν(C–N)) [20,25], and 1070 cm^{-1} (ν(C=S)) [26,27], evidencing incorporation of the thioamide moiety.

The scanning electron microscope (SEM) image in Fig. 2**d** shows that BDTA exhibits a typical flake-like aggregated morphology, with relatively uniform particle distribution and sizes mainly concentrated in the range of 1–5 μm. Thermogravimetric analysis (Fig. 2**e**) indicates robust thermal stability, with major mass loss occurring only above ~170 °C—higher than many organosulfur cathodes [28]. In addition, the powder X-ray diffraction pattern (**Figure S1**) exhibits sharp reflections at 2θ = 16.54°, 23.09°, 24.06°, 25.42°, and 26.59°, confirming the crystalline nature of BDTA.

Electrochemical performance of the as-prepared BDTA was comprehensively evaluated. As illustrated in Fig. 3**a**, the cyclic voltammetry (CV) curve of BDTA was tested within the voltage range of 1.2–3.4 V vs. Li^{+}/Li. During the first discharge, four distinct voltage plateaus appear at approximately 2.3 V, 2.09 V, 1.53 V and 1.37 V, corresponding to a multistep reduction process involving successive redox-active centers. In which, the reduction peak at 2.09 V is sharp, indicative of a well-defined two-phase reaction process. Accordingly, three oxidation features emerge within 2.2–2.4 V: a weak shoulder at 2.22 V, followed by two adjacent, sharper peaks at 2.33 V and 2.39 V, indicating that the oxidation reaction exhibits stronger delocalized characteristics [29]. Fig. 3**b** presents the galvanostatic charge–discharge profiles of the BDTA cathode at 0.1 C (1 C = 546 mA g^{-1}) for the 1st, 2nd, 5th, and 10th cycles. An initial irreversible capacity loss is observed, which is commonly associated with solid electrolyte interphase (SEI) formation. The subsequent cycles (the 2nd to 10th cycles) exhibit good overlapping of the curves and a stable capacity output, indicating that the electrode reaction achieves reasonable reversibility and interfacial stability in the initial cycling period. On discharge, a pronounced slope

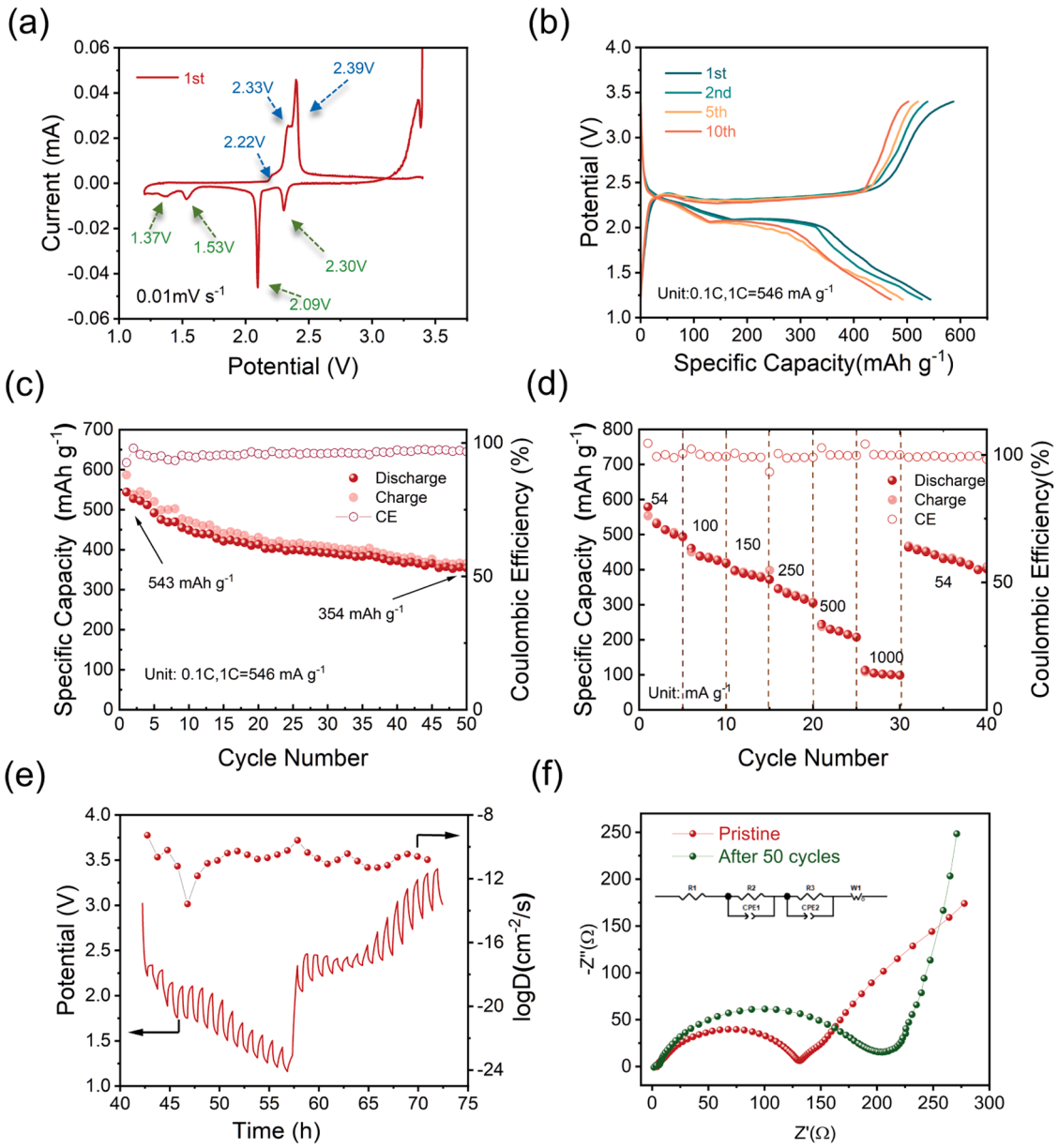

Fig. 3. (a) CV curves of BDTA at scan rates ranging from 0.01 mV s^{-1}; (b) Charge/discharge profiles of Li || BDTA cell at different cycle numbers under a current density of 0.1 C; (c) Cycling performance of the Li || BDTA cell at 0.1 C; (d) Rate performance of the Li || BDTA cell at various current densities; (e) GITT profile of BDTA and the corresponding lithium-ion diffusion coefficients; (f) Nyquist plots showing the interfacial resistance of BDTA before and after 50 cycles.

appears at 2.25 V vs. Li^+/Li, followed by a clear plateau near 2.0 V; a second sloping region emerges around 1.53 V and gradually declines to 1.2 V, which is consistent with stepwise Li^+ insertion and multielectron reactions. On charge, a broad plateau is observed near 2.3 V, with a stepwise rise between 2.7–3.3 V, which is in good agreement with the CV features in Fig. 3**a**. In addition, the BDTA electrode delivers a reversible capacity of ~540 mAh g^{-1}, that is close to the theoretical value, highlighting a high active-site utilization and favorable kinetics. Cycling stability performance was examined at 0.1 C for 50 cycles. The cycling performance in Fig. 3c shows that the BDTA electrode delivered a discharge capacity of ~354 mAh g^{-1} after 50 cycles, retaining 65.2 % of its capacity. The observed capacity fade may be attributed to interfacial side reactions or partial dissolution of the active material. Nevertheless, the coulombic efficiency was consistently close to 100 %, indicating that the charge storage chemistry itself is highly reversible. In contrast, at 0.1 C, the Li || DPyDS battery exhibits pronounced first-cycle polarization and a low initial coulombic efficiency, delivering a reversible capacity of ~200 mAh g^{-1} (**Figure S3a**). Moreover, during subsequent cycling, the capacity continues to decline (**Figure S3b**), and both capacity retention and coulombic efficiency are clearly inferior to BDTA, resulting in overall performance markedly worse than BDTA, consistent with the preceding theoretical calculations in Fig. 1. To be noted, capacities for BDTA electrode shows relatively higher capacity in comparation with other organosulfur cathodes (Table S1). The primary contribution of this work is the establishment of a fundamentally new C=S redox mechanism. The achieved performance, notably the high specific capacity, directly validates this chemistry and establishes a robust platform for future development.

The rate capability of the electrode was assessed at various current densities ranging from 54 to 1000 mA g^{-1} (Fig. 3**d**). As can be observed, the electrode maintains a capacity of 546.5 mAh g^{-1} at 54 mA g^{-1}, and retains 432.9, 398.1, 377.7, 332, 229.7 and 101.7 mAh g^{-1} at 100, 150, 250, 500, and 1000 mA g^{-1}, respectively. When the current density is returned to 54 mA g^{-1}, the capacity recovers to 503 mAh g^{-1},

demonstrating excellent structural resilience and fast kinetics [30]. In contrast, the DPyDS cathode exhibited significantly lower capacities of 315.7, 101.3, 79.6, 71.4, 56.4, and 37.7 mAh g^{-1} under the same current density range **(Figure S3c)**, with only a marginal recovery to 92 mAh g^{-1} upon returning to 50 mA g^{-1}. Moreover, the DPyDS electrode suffered from a low coulombic efficiency of only ~70 % throughout the rate test, indicating severe side reactions such as polysulfide shuttling and active material dissolution. Lithium-ion diffusion behavior was investigated using Galvanostatic Intermittent Titration Technique (GITT) [31]. As shown in Fig. 3**e** and **Figure S3d**, the BDTA and DPyDS electrodes exhibit typical staircase voltage responses during intermittent current pulses, and the calculated Li^+ diffusion coefficients (D_{Li^+}) vary from ~10^{-9} to 10^{-14} cm^2 s^{-1}, depending on the state of charge [32].

Electrochemical impedance spectroscopy (EIS) was used to monitor interfacial evolution after cycling (Fig. 3**f**). After 50 cycles, the high-/mid-frequency semicircle enlarges and the charge-transfer resistance R_{ct} increases from 125 to 200 Ω (ΔR_{ct}=75Ω), indicating only moderate interfacial growth and overall interfacial stability. Concurrently, the low-frequency tail becomes steeper, consistent with reduced diffusion impedance and improved Li^+ transport after cycling. In stark contrast, the DPyDS electrode exhibits a much larger initial R_{ct} of 880 Ω, which further increases to 1100 Ω after only 40 cycles (Figure S4). The significantly higher R_{ct} values and more substantial interfacial growth observed for DPyDS underscore the superior interfacial stability and charge-transfer kinetics of the BDTA cathode, consistent with its better cycling performance and higher coulombic efficiency.

The redox mechanism of BDTA electrode during cycling in lithium-ion batteries was further elucidated by in situ FTIR spectroscopy and ex situ XPS. The galvanostatic potential–time profile (Fig. 4**a**) serves as a reference for assigning the time-correlated spectral variations. The 2D color-filled contour maps derived from in situ FTIR spectra in Figs. 4**b** and 4**c** reveal the dynamic changes of key functional groups throughout the lithiation/delithiation processes. As shown, a distinct absorption band located at 1070 cm^{-1}, corresponding to the C=S stretching vibration, gradually decreases in intensity during discharge, indicating progressive cleavage of the thiocarbonyl bond and its coordination with Li^+ to generate C-S-Li group. Upon subsequent charging, the C=S signal reappears with partial intensity recovery, reflecting reversible electrochemical oxidation of C–S to regenerate C=S, suggesting a reversible C=S ↔ C–S transformation pathway mediated by Li^+ insertion/extraction. Additionally, a vibrational band at ~1270 cm^{-1}, associated with the C–N stretching mode, exhibits a reversible bathochromic shift (red-shift) during in-situ FTIR. This behavior is attributed to electronic delocalization effects triggered by the redox activity of neighboring C=S/C–S motifs, which modulate the resonance hybridization of the adjacent C–N bond. Specifically, during discharge, the reduction of C=S to C–S extends π-electron delocalization toward the C–N unit [33], effectively increasing its bond order and resulting in a transition from C–N to $C = N$ character. This resonance-assisted transformation is consistent with the observed FTIR shifts and supports a redox-coupled bond reorganization mechanism. Interestingly, although the N–H group does not directly participate in the redox reaction, its stretching vibration (~3300 cm^{-1}) shows noticeable intensity fluctuations throughout the charge–discharge process. This spectral evolution is likely a consequence of redox-induced molecular conformation changes, which perturb the local bonding environment of the N–H group and alter its vibrational behavior [34].

To complement the FTIR findings, ex situ XPS analysis was conducted at different electrochemical states. The C_{1s} spectra in Fig. 4d exhibit components corresponding to C–C (~284.8 eV), C=S (~285.9 eV), and C–N (~287.1 eV). Upon discharge to 1.2 V, the C=S signals diminish in intensity, indicating lithiation-induced bond weakening or electronic rearrangement. These peaks partially recover after charging to 3.4 V, confirming the reversibility of the redox-induced structural changes. The S_{2p} spectra in Fig. 4**e** show that the BDTA electrode exhibits only a pair of doublet at 162.28 eV, corresponding to sulfur in C=S. During discharge, a significant weakening of the C=S signal is observed. Meanwhile a C-S signal centered at 165.23 eV, indicating the transition from C=S to C-S. Upon charging, a pronounced recovery of the C=S signal is observed, concomitant with the attenuation of the C–S signal, evidencing the reversible transformation between C=S and C–S bonds during the electrochemical process. The N 1 s spectra in Fig. 4**f** reveal two peaks at ~399.8 eV and ~400.4 eV, corresponding to C—N and N—H, respectively. During discharge, the C—N signal weakens, while the $C = N$ component increases, reflecting a shift in the electron density distribution around nitrogen. These spectral changes also partially recover upon charging, further corroborating the reversible nature of the redox process involving nitrogen-adjacent moieties.

The lithiation mechanism and the associated Gibbs free-energy landscape were computed with Gaussian, and the results are shown in Fig. 4***g*** As shown, at the initial lithiation step, Li^+ preferentially coordinates to the thioamide C=S motif, forming a chelating S···Li···N interaction with the vicinal N atom. The second Li^+ occupies the C=S site opposite to the first and likewise forms an S···Li···N chelate. Subsequently, the third and fourth Li^+ ions bind to the remaining thioamide sites, yielding a multi-site, cooperatively coordinated configuration. Consistent with this sequence, the Gibbs free energy (ΔG) decreases monotonically along the lithiation pathway—from BDTA (0 eV) to BDTA(Li) (−4.04 eV), $BDTA(Li)_2$ (−7.41 eV), $BDTA(Li)_3$ (−9.91 eV), and $BDTA(Li)_4$ (−15.32 eV). This progressive drop in ΔG indicates that each step is thermodynamically favorable and aligns with the average reaction voltage decreasing from 3.2 to 1.2 V, thereby corroborating a reversible four-electron/four-site storage mechanism.

The morphological evolution of the BDTA cathode during cycling was systematically investigated by Scanning Electron Microscope (SEM). As shown in **Figure S5a**, the pristine electrode exhibits a block-like agglomerated morphology with tightly bound particles and a rough surface, and the intimate particle–binder–carbon contact formed during electrode preparation is expected to facilitate Li^+ transport. Upon discharge (**Figure S5b**), numerous sheet-like crystalline domains emerge, revealing a pronounced phase transformation and the formation of highly ordered crystalline products, which is likely driven by the cleavage of C=S bonds in the thioamide moieties followed by Li^+ coordination. During subsequent charging (**Figure S5c**), the electrode surface becomes smoother with refined and uniformly distributed particles, while the sheet-like crystals almost vanish, indicating that the discharge products undergo reversible electrochemical oxidation, partially restoring the original structure and confirming the good reversibility of the BDTA electrode.

To demonstrate molecular generality, we extended this thioamide-based redox motif from a benzene scaffold to a naphthalene framework by evaluating 1,4-naphthalenedicarbothioamide (NDTA) as a cathode (**Figure S6**). As can be observed, NDTA delivers an initial discharge capacity of 407.2 mAh g^{-1} at 0.1 C (≈93 % of the theoretical value) and retains 211.4 mAh g^{-1} after 50 cycles. It can be hypothesize that its lithiation mechanism mirrors that of BDTA (**Scheme S1**), proceeding via stepwise Li^+ coordination at C=S sites with successive electron transfers.

To gain further insight into the reaction mechanism of NDTA, ex situ FTIR measurements were performed on electrodes at different potentials (**Figure S7b**). Particular attention was paid to the C=S stretching vibration, In the pristine electrode, a distinct C=S stretching band appears near ~1070 cm^{-1}, characteristic of the thiocarbonyl moiety. As the cell discharges, this band progressively weakens and nearly disappears at 1.2 V, indicating significant reduction and cleavage of the C=S bond. Meanwhile, the 1000–1200 cm^{-1} region exhibits broadening and intensity redistribution, consistent with the formation of Li-thiolate (C–S–Li) species and related reduced intermediates. These spectral changes confirm that lithiation triggers nucleophilic attack by Li^+ at the thiocarbonyl sulfur, collapsing the double bond.

Furthermore, ex situ XPS analysis provided key evidence supporting the proposed redox mechanism **(Figure S7c-d)**. In the pristine material,

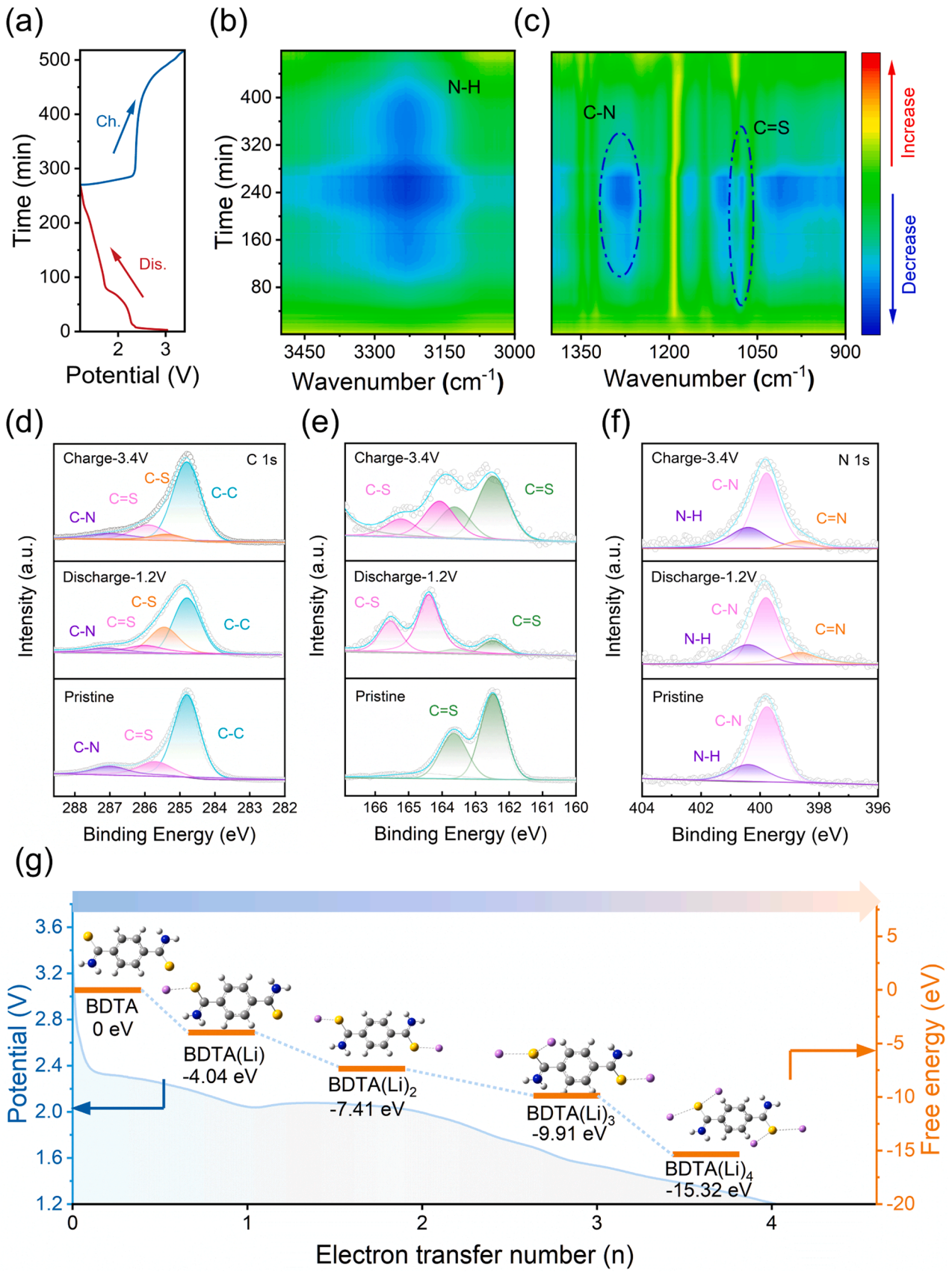

Fig. 4. (a) Charge–discharge voltage–time profiles of the BDTA cell at 0.2 C; (b, c) Operando FTIR spectra corresponding to the high-wavenumber (b) and low-wavenumber (c) regions; (d–f) High-resolution XPS spectra of C 1 s (d), S 2p (e), and N 1 s (f) at different electrochemical states (pristine, discharged at 1.2 V, and charged at 3.4 V). (g) Calculated energy diagram and redox potential of BDTA, and schematic diagram of the BDTA Discharge Process.

the C 1 s spectrum shows contributions from aromatic C—C (284.7 eV), C=S-bonded carbon (286.2–286.6 eV), and C—N functionalities. Upon discharging to 1.2 V, the C=S-derived carbon peak diminishes markedly, accompanied by the emergence of a new component at slightly lower binding energies (285.6–286.0 eV) corresponding to reduced C-S-Li species. The aromatic C—C peak remains unchanged, confirming that the naphthalene backbone is electrochemically stable. During charging to 3.4 V, the reduced C-S component weakens and the C=S peak is restored, demonstrating reversible re-formation of the thiocarbonyl group with only minor residual C-S features. The S 2p spectrum provides decisive evidence for the sulfur redox process. In the pristine state, the main S $2p_{3/2}2p_{1/2}$ doublet at ~162–163 eV corresponds to thiocarbonyl sulfur. During discharge, this peak significantly decreases, while a new reduced sulfur doublet at 160.5–161.5 eV appears, assigned to thiolate (C–S–Li) species. When recharged to 3.4 V, the thiolate signal diminishes and the C=S doublet is largely restored, confirming reversible sulfur reoxidation and thiocarbonyl regeneration.

Notably, the longer conjugated backbone of NDTA is accompanied by poorer cycling stability, plausibly due to its higher polarizability that increases solubility and accelerates capacity fading. These results confirm that thioamide-centered organic electroactive molecules can be extendable to naphthalene or other derivatives. Looking ahead, targeted molecular design that tunes conjugation length, substituents, and intermolecular interactions could deliver further improvements in specific capacity, cycling stability, and rate capability.

3. Conclusion

In this work, we establish thioamide C=S–centered redox electrochemistry as an effective multielectron chemistry for organic Li-ion cathodes, validated with BDTA. The BDTA electrode operates near its theoretical capacity (~543 mAh g^{-1}) and maintains ~354 mAh g^{-1} after 50 cycles at 0.1 C with high coulombic efficiency and a robust rate response. Operando FTIR and ex situ XPS directly track reversible C=S ⇄ C–S transformations, while Gaussian calculations resolve a stepwise four-electron Li^+-binding sequence accompanied by a monotonic drop in Gibbs free energy, linking molecular mechanism to device-level behavior. GITT and EIS further indicate state-dependent Li^+ transport and manageable interfacial evolution under practical cycling. Extension to a naphthalene analogue (NDTA) confirms the molecular generality of this aromatic thioamide motif. Our work provides a new, mechanism-vetted option within organosulfur electrode materials, expanding the molecular design space beyond conventional motifs and providing a clear framework—centered on reversible C=S redox—for achieving high-capacity, reversible organic cathodes.

CRediT authorship contribution statement

Tingting Jiang: Writing – original draft, Methodology, Investigation, Formal analysis, Data curation. **Wenwen Deng:** Writing – review & editing, Funding acquisition, Conceptualization. **Qingqing Ma:** Methodology. **Chunxian Guo:** Resources. **Zhong Jin:** Writing – review & editing, Funding acquisition, Conceptualization.

Declaration of competing interest

The authors declare that they have no known competing financial interests or personal relationships that could have appeared to influence the work reported in this paper.

Acknowledgment

This work was funded by The Natural Science Foundation of the Jiangsu Higher Education Institutions of China (23KJB150032, 24KJA15004), National Natural Science Foundation of China (U25A20628, 22561160129, 22479074, 22475096), the Equipment Pre-Research and Ministry of Education Joint Fund (8091B02052407), the Fundamental Research Program Key Project of Jiangsu Province (BK20253008), the Science and Technology Major Project of Jiangsu Province (BG2024013), the Scientific and Technological Achievements Transformation Special Fund of Jiangsu Province (BA2023037), the Academic Degree and Postgraduate Education Reforming Project of Jiangsu Province (JGKT24_C001), the Key Core Technology Open Competition Project of Suzhou City (SYG2024122), the Open Research Fund of Suzhou Laboratory (SZLAB-1308–2024-TS005), and the Chenzhou National Sustainable Development Agenda Innovation Demonstration Zone Provincial Special Project (2023sfq11).

Supplementary materials

Supplementary material associated with this article can be found, in the online version, at doi:10.1016/j.ensm.2025.104784.

Data availability

Data will be made available on request.

References

[1] W. Guo, D. Wang, Q. Chen, Y. Fu, Advances of organosulfur materials for rechargeable metal batteries, Adv. Sci. 9 (2022) 2103989.
[2] A. Bhargav, M.E. Bell, J. Karty, Y. Cui, Y. Fu, A class of organopolysulfides as liquid cathode materials for high-energy-density lithium batteries, ACS Appl. Mater. Interfaces 10 (2018) 21084–21090.
[3] A. Bhargav, S.V. Patil, Y. Fu, A phenyl disulfide@CNT composite cathode for rechargeable lithium batteries, Sustain. Energy Fuels 1 (2017) 1007–1012.
[4] D. Wang, Y. Si, W. Guo, Y. Fu, Long cycle life organic polysulfide catholyte for rechargeable lithium batteries, Adv. Sci. 7 (2020) 1902646.
[5] M. Armand, J.M. Tarascon, Building better batteries, Nature 451 (2008) 652–657.
[6] M. Wu, Y. Cui, A. Bhargav, Y. Losovyj, A. Siegel, M. Agarwal, Y. Ma, Y. Fu, Organotrisulfide: a high capacity cathode material for rechargeable lithium batteries, Angew. Chem. Int. Ed. 55 (2016) 10027–10031.
[7] Y. Liang, Z. Tao, J. Chen, Organic electrode materials for rechargeable lithium batteries, Adv. Energy Mater. 2 (2012) 742–769.
[8] H. Wu, K. Wang, Y. Meng, K. Lu, Z. Wei, An organic cathode material based on a polyimide/CNT nanocomposite for lithium ion batteries, J. Mater. Chem. A 1 (2013) 6366–6372.
[9] S.J. Visco, C.C. Mailhe, L.C. De Jonghe, M.B. Armand, A novel class of organosulfur electrodes for energy storage, J. Electrochem. Soc. 136 (1989) 661–664.
[10] T. Maddanimath, Y.B. Khollam, M. Aslam, I.S. Mulla, K. Vijayamohanan, Self-assembled monolayers of diphenyl disulphide: a novel cathode material for rechargeable lithium batteries, J. Power Sources 124 (2003) 133–142.
[11] P. Yu, J. An, Z. Wang, Y. Fu, W. Guo, An organic molecular cathode composed of naphthoquinones bridged by organodisulfide for rechargeable lithium battery, Small 20 (2024) 2308881.
[12] Z. Wang, Q. Fan, Y. Si, W. Guo, Y. Fu, A self-regulatory organosulfur copolymer cathode towards high performance lithium-sulfur batteries, Energy Storage Mater. 58 (2023) 222–231.
[13] L.-P. Hou, X.-Q. Zhang, N. Yao, X. Chen, B.-Q. Li, P. Shi, C.-B. Jin, J.-Q. Huang, Q. Zhang, An encapsulating lithium-polysulfide electrolyte for practical lithium–sulfur batteries, Chem. 8 (2022) 1083–1098.
[14] S.-H. Chung, C.-H. Chang, A. Manthiram, Progress on the critical parameters for lithium–sulfur batteries to be practically viable, Adv. Funct. Mater. 28 (2018) 1801188.
[15] X. Lv, W. Guo, J. Song, Y. Fu, Dynamic 1T-2H mixed-phase MoS_2 enables high-performance li-organosulfide battery, Small 18 (2022) e2105071.
[16] Z. Shadike, S. Tan, Q.-C. Wang, R. Lin, E. Hu, D. Qu, X.-Q. Yang, Review on organosulfur materials for rechargeable lithium batteries, Mater. Horiz. 2 (2021) 471–500.
[17] X. Zuo, K. Chang, J. Zhao, Z. Xie, H. Tang, B. Li, Z. Chang, Unique chemistry of thiuram polysulfides enables energy dense lithium batteries, J. Mater. Chem. A 4 (2016) 51–58.
[18] S. Dixon, R.J. Whitby, Efficient synthesis of thioamide terminated molecular wires, Tetrahedron Lett. 47 (2006) 8147–8150.
[19] G. Cao, R. Duan, X. Li, Controllable catalysis behavior for high performance lithium sulfur batteries: from kinetics to strategies, Energy Chem. 5 (2023) 100096.
[20] S. Karak, H. Singh, A. Biswas, S. Paul, S. Manna, Y. Nishiyama, B. Pathak, A. Banerjee, R. Banerjee, Lithiophilic dibenzamide linkages to impart lithium storage capacity in porous polybenzamides, J. Am. Chem. Soc. 146 (2024) 20183–20192.
[21] H. Wang, G. Liu, W. Zhou, Y. Wang, X. Dong, High-potential and stable organic cathode for rechargeable batteries with fast-charging and wide-temperature adaptability, Angew. Chem. Int. Ed. (2024) e202416874.

[22] J.-N. Zhang, Q. Li, Y. Wang, J. Zheng, X. Yu, H. Li, Dynamic evolution of cathode electrolyte interphase (CEI) on high voltage $LiCoO_2$ cathode and its interaction with li anode, Energy Storage Mater. 14 (2018) 1–7.
[23] H. Lyu, C.J. Jafta, I. Popovs, H.M. Meyer, J.A. Hachtel, J. Huang, B.G. Sumpter, S. Dai, X.-G. Sun, A dicyanobenzoquinone based cathode material for rechargeable lithium and sodium ion batteries, J. Mater. Chem. A 7 (2019) 17888–17895.
[24] E. Gopi, E. Gravel, E. Doris, Triphenylbismuth dichloride-mediated conversion of thioamides to nitriles, Eur. J. Org. Chem. (2019) 4043–4045, 2019.
[25] T. Song, Q. Ma, B. Wang, X. Zhang, Y. Wang, H. Xiong, High-capacity and long-life cathode constructed solely by carbon dots for aqueous zinc-ion batteries, Angew. Chem. Int. Ed. (2025).
[26] A. Tao, K. Zhang, X. Ma, X. Song, J. Liang, Y. Wang, Y. Liu, L. Jin, Z. Tie, Z. Jin, Building lithium-polycarbonsulfide batteries with high energy density and long cycling life, ACS Energy Lett. 8 (2023) 79–89.
[27] G.B. Ferreira, N.M. Comerlato, J.L. Wardell, E. Hollauer, Vibrational spectra of tris (dmit) complexes of main group metals: infrared, raman and ab initio calculations, Spectrochim. Acta. A. Mol. Biomol. Spectrosc. 61 (2005) 2663–2676.
[28] H. Liu, F. Zhu, Y. Zhang, Y. Liu, Y. Zhang, W. Deng, G. Zou, H. Hou, X. Ji, Synergistic regulation of multi-interface chemistry by functional carbon dots for high-performance composite solid electrolytes, Angew. Chem. Int. Ed. 64 (2025) e202505230.
[29] T. Imai, T. Amaya, Characterization of cyclic [*n*]spirobifluorenylene compounds and electron delocalization in their radical cation species, Chem. – Asian J. 20 (2025) e202500320.
[30] D.-Y. Wang, Y. Si, J. Li, Y. Fu, Tuning the electrochemical behavior of organodisulfides in rechargeable lithium batteries by N-containing heterocycles, J. Mater. Chem. A 7 (2019) 7423–7429.
[31] X. Song, Q. Yu, J. Li, Z. Wu, Y. Xing, Y. Wang, L. Qin, H. Sun, Z. Tie, J. Ma, Z. Jin, In-situ electro-polymerization of aromatic diimide bridged N-phenylcarbazole as high-voltage cathode materials for long-lasting cationic and anionic co-storage batteries, Chem. Eng. J. 512 (2025) 162419.
[32] X. Qi, F. Yang, P. Sang, Z. Zhu, X. Jin, Y. Pan, J. Ji, R. Jiang, H. Du, Y. Ji, Y. Fu, L. Qie, Y. Huang, Electrochemical reactivation of dead Li_2S for Li−S batteries in non-solvating electrolytes, Angew. Chem. Int. Ed. 62 (2023) e202218803.
[33] G. Zhang, A. Ji, D. Chen, Origin of blue and red shifts of C–H and C–N stretching vibrations in formamide–HF/H_2O/H_2S/NH_3 complexes, J. Mol. Struct. Theochem. 853 (2008) 89–96.
[34] S. Mishra, H.-Q. Nguyen, Q.-R. Huang, C.-K. Lin, J.-L. Kuo, G.N. Patwari, Vibrational spectroscopic signatures of hydrogen bond induced NH stretch–bend fermi-resonance in amines: the methylamine clusters and other N–H···N hydrogen-bonded complexes, J. Chem. Phys. 153 (2020) 194301.